Chapter 20

The Outer Heliosphere

The **Aims** of this chapter are to, first, introduce the physics of the distant solar wind and its interaction with the solar wind and, second, to complete our survey of the solar system.

The outer heliosphere, where the solar wind meets and interacts with the local interstellar medium, represents the current boundary between space physics and astrophysics and also the plasma boundary of our solar system. Study of the outer heliosphere requires the consideration of both kinetic and MHD physics. The kinetic physics is related to pickup ions, heating, turbulence, acceleration of energetic particles called the "anomalous cosmic rays", and the production of radio emissions. The fluid or MHD physics involves the macroscopic plasma structures and boundaries in the outer heliosphere (e.g., the termination shock and heliopause), evolved CIRs and CMEs called "global merged interaction regions", and the effects of pickup ions in slowing and heating the flow. The characteristics of the local interstellar medium are also of interest, especially remote sensing of the properties thereof. Remember that the scales are very large. The nearest star is about 4 light-years or 1 parsec away, with 1 lightyear being about $63,000$ AU, and long-period comets in the Oort cloud having semi-major axes of about $100,000$ AU. As justified below, the plasma boundary of our solar system is likely about $120 - 160$ AU away, some $3 - 4$ times more distant than the known planets but much closer than the Oort cloud.

The termination shock of the solar wind was recently crossed by spacecraft: Voyager 1 on 16 December 2004 and Voyager 2 around 1 September 2007. It appears to be a relatively standard fast-mode shock, but with an unusually large role for the pickup ions. The first papers on the Voyager 2 results, the first spacecraft to probe the shock with a functioning plasma instrument, came out in Nature in 2008.

This Lecture proceeds by summarising the properties of the solar wind and interstellar pick-up ions, discussing the remotely determined properties of the "very local interstellar medium" (VLISM), describing the global plasma boundaries and structures and estimating their likely locations based on various models, discussing the termination shock and global simulations of the outer heliosphere, and then joining these seemingly disparate concepts into a discussion of radio emissions that seem to be triggered by travelling solar disturbances in the vicinity of the heliopause.

Expected Learning Outcomes. You are expected to be able to

- Describe the characteristic plasma boundaries expected as a result of the solar wind's interaction with the local interstellar medium.
- Describe the physics of these plasma boundaries.

- Describe ways to investigate the characteristics of the local interstellar medium from inside the solar system.
- Describe and explain ways to predict that the termination shock is nearby and that a spacecraft has crossed the shock.
- Describe the 2-3 kHz radio emissions observed by the Voyager spacecraft and current models for explaining them.

20.1 Recap of solar wind physics and interstellar pick-up ions

Standard Parker-type solar wind theories predict that the radial and ϕ components of the magnetic field should vary approximately as R^{-2} and R^{-1} for constant solar wind speed, where R is the heliocentric distance (see Eqs. (6.20) and (6.24)). Accordingly, the ϕ component dominates in the outer heliosphere and the magnetic field becomes increasingly perpendicular to the solar wind velocity, on average. In addition, the magnetic field energy density falls off as R^{-2} at large R, similar to the ram kinetic energy of the solar wind. These variations are consistent with Figure 11.9. They also mean that the Alfven Mach number M_A is essentially constant for large R. On the other hand, the fast mode and sonic Mach numbers decrease at large R as the heating by pickup ions causes the sound speed for the overall fluid to increase with R.

The solar wind plasma density decreases as R^{-2} (Figure 11.8), as expected for global mass conservation in radial flows and from standard Parker theory, whence the plasma frequency $f_p \propto R^{-1}$ on average. The solar wind speed is observed and predicted to be almost constant with R, at least until mass-loading by pick-up ions becomes important and the flow is slowed (Figure 11.14). The ordinary solar wind ions and electrons are expected to cool adiabatically (they are moving into an expanding volume), although heating by CIR shocks is important from a few to about 20 AU, and heating by MHD turbulence is likely important too.

As discussed in Chapter 11, interstellar pick-up ions come from interstellar neutrals which enter the heliosphere, charge-exchange with solar wind protons, start off essentially at zero velocity relative to the Sun, and are then accelerated by the solar wind convection electric field to reach a large gyrospeed $\sim 2v_{sw}\sin\theta$ (θ is the angle between $\mathbf{v}_{sw}$ and $\mathbf{B}_{sw}$), forming a ring-beam distribution with very large effective temperature relative to the solar wind ions. The pick-up ions then $\mathbf{E}\times\mathbf{B}$ drift out of the heliosphere with the solar wind, as well as moving parallel to $\mathbf{B}_{sw}$ (with very low speed) and performing their gyromotion. The energy required to create this gyromotion comes from the convection electric field and so from the solar wind flow itself. Accordingly, the solar wind is effectively heated and slowed by the charge-exchange and pick-up of these interstellar neutrals. Evidence for this heating and slowing is provided by Figures 11.13 and 11.14, respectively.

Pick-up ions are predicted theoretically to have significant effects on the details of the global outer heliosphere, affecting for instance the locations and perhaps structures of the characteristic plasma boundaries like the termination shock and the heliopause, as reviewed by Zank [1999]. Additionally, these pick-up ions are accelerated at the termination shock, perhaps forming the so-called "anomalous cosmic ray component" observed at Earth and throughout the heliosphere.

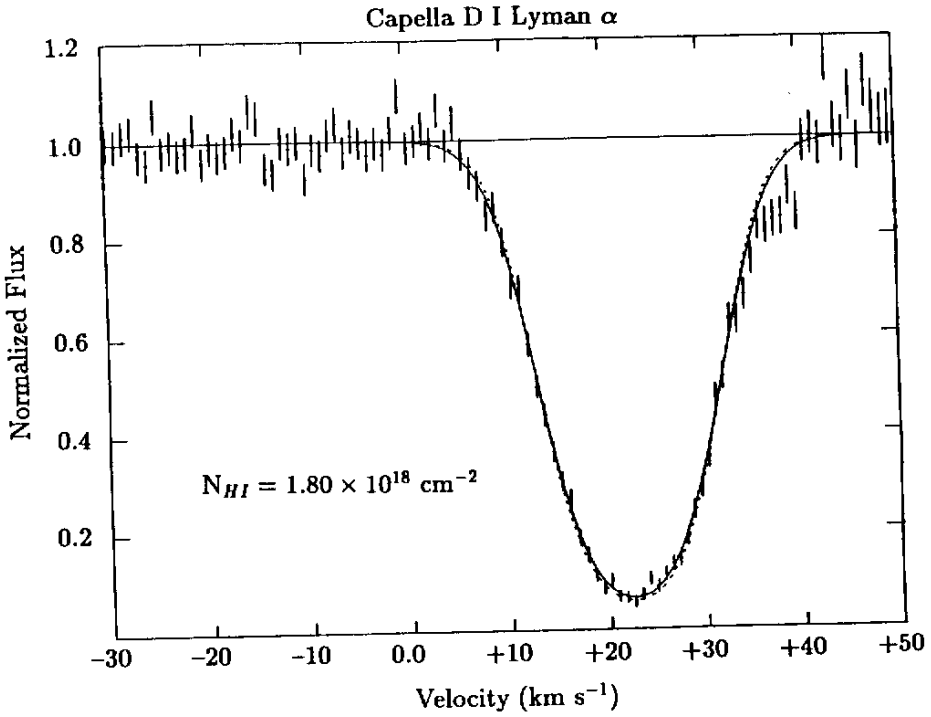

Figure 20.1: Hubble GHRS spectrum of Capella [Linsky et al., 1993; Lallement, 1993].

20.2 Remotely determined properties of the VLISM

Estimates for the average properties of the VLISM can be obtained remotely using a number of methods: (1) the Doppler shift and intensity of solar radiation that is backscattered to observers near 1 AU or in the outer heliosphere, (2) radiation from other stars that has superposed absorption or emission lines, (3) interstellar pick-up ions, (4) interstellar neutral atoms detected directly, and (5) the properties of radio emissions from the solar wind-VLISM interface. The properties of the local interstellar medium on a larger scale (several parsecs) can also be estimated by studying the absorption and emission features of light from nearby stars.

Figure 20.1 [Linsky et al., 1993; Lallement, 1993] is a Hubble Space Telescope GHRS Lyman-alpha spectrum of the star Capella (12.5 pc distant) showing the absorption line due to the local interstellar medium between the Sun and Capella. The spectrum indicates that there is a single well-defined "cloud" of interstellar material between the Sun and Capella, having a line-of-sight velocity difference of about 23 km s^{-1}. This interpretation is consistent with absorption features along different lines of sight to other nearby stars [Lallement, 1993]. There is evidence for multiple clouds, in other directions, in the Sun's local region of the interstellar medium [Frisch, 2003].

Backscattering of solar Lyman-alpha radiation by hydrogen and helium atoms leads to the estimates in Table 1 for the number density, temperature, and relative speeds of these species. The table also contains estimates derived from direct detection of neutral helium atoms [Witte et al., 1996] and of pick-up ions, as summarised by Zank [1999].

Note that the velocity of the VLISM relative to our solar system is well de-

Technique	$n_H(10^{-2}\mathrm{cm}^{-3})$	$v_H(\mathrm{kms}^{-1})$	$T_H(K)$	$n_{He}(10^{-2}\mathrm{cm}^{-3})$	$v_{He}(\mathrm{kms}^{-1})$	$T_{He}(K)$
VLISM UV	–	-26	–	–	–	
SW UV	10 ± 4	$18 - 21$	8000	$0.5 - 1.4$	$19 - 24$	8000
Direct	–	–	–	$1.4 - 1.7$	25	7000 ± 600
Pick-up	11 ± 3	–	–	$0.9 - 1.5$	–	$4800 - 7200$

Table 20.1: The number densities, flow speeds, and temperatures inferred for neutral hydrogen and helium atoms in the VLISM using various techniques. "UV" refers to techniques using UV radiation either in the VLISM or solar wind (SW), while "direct" refers to Witte et al.'s [1996] direct detection method and "pick-up" refers to interstellar pick-up ions detected in the solar wind.

termined, that hydrogen atoms appear to be slowed preferentially on entering the heliosphere, that the temperatures of the interstellar hydrogen and helium atoms are consistently ≈ 8000 K, and that the total neutral number densities are $\approx 0.13 \pm 0.04$ cm^{-3}. Calculations using versions of the Saha equation (which relates together the ionization potential, thermal temperature, and number densities of plasma constituents and neutrals) then yield the expected electron number density in the VLISM: $0.03 < n_e < 0.15$ cm^{-3}. The corresponding limits on the plasma frequency are then

$$1.5 < f_p < 3.5\mathrm{kHz} \ . \tag{20.1}$$

These constraints on f_p will be important in understanding the radio emissions observed and generated in the outer heliosphere (Section 20.5).

20.3 Nature and location of global plasma boundaries and structures in the outer heliosphere

The plasma boundaries in the outer heliosphere are illustrated schematically in Figure 20.2. The solar wind is supersonic and superalfvenic and its ram pressure varies as R^{-2}, thereby eventually becoming less than the effective pressure (the sum of ram, thermal and magnetic pressures - see Eq. (19.4), for instance) of the VLISM. Note also that $P_{th}(R)$ should also vary approximately as R^{-2} too, despite the addition of pickup ions, since $P_{th}(R) = n_{core}(R)k_B T_{core}(R) + n_{pi}(R)k_B T_{pi}(R)$ with both the core solar wind density $n_{core}(R)$ and the pickup ion number density $n_{pi}(R)$ varying approximately as R^{-2} as the solar wind expands into a larger volume. Accordingly, the solar wind must undergo a shock transition in its interaction with the VLISM. This shock, called the "termination shock", is where the solar wind is compressed, heated, deflected, and made subalfvenic.

As described in the last section, the VLISM gas and plasma are believed to flow at a speed of 26 km s^{-1} relative to the Sun and the heliosphere. If this speed is supersonic or superalfvenic in the VLISM plasma, then there will be a (outer) "bow shock" for our solar system. This flow is supersonic ($C_s \sim 8$ km s^{-1}), but it is presently unknown experimentally whether the VLISM flow is superalfvenic. Current theoretical estimates predict that $M_A \sim 1.0$.

The heliopause, the other major plasma boundary, is a tangential discontinuity between the shocked solar wind and the possibly shocked VLISM plasma. It is analogous to planetary magnetopauses and ionopauses, and to pressure-balanced structures in the solar wind (cf. Lectures 14, 18, and 19). To recap, from the point of view of MHD theory the plasmas remain separate because (1) they are highly conducting with frozen-in fields that resist encroachment by the field of

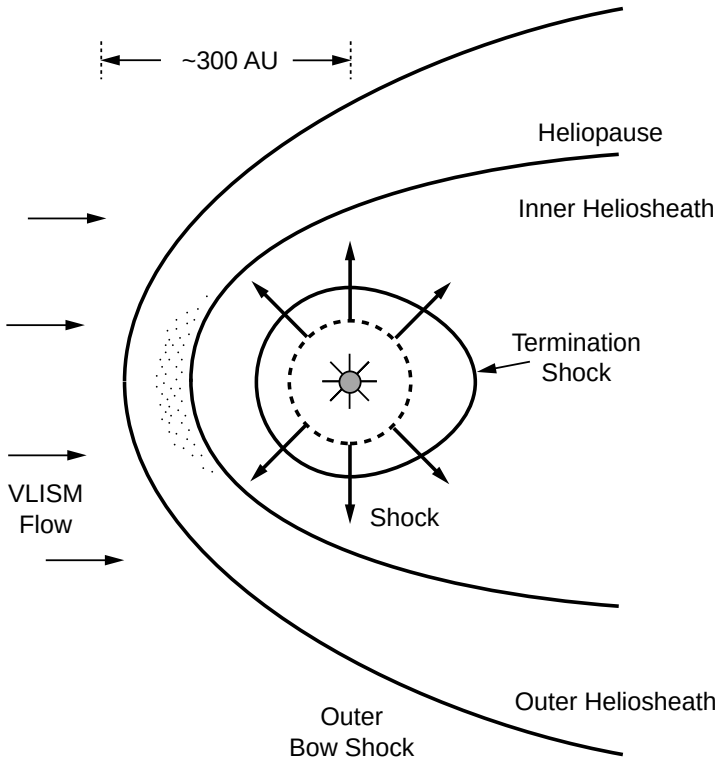

Figure 20.2: Schematic of the plasma boundaries expected in the outer heliosphere.

another region and (2) the gyromotion of individual charged particles leads to a current in the interface region which experiences a $\mathbf{J} \times \mathbf{B}$ force that separates the plasmas. From the viewpoint of kinetic theory the plasmas remain separate because the particles from the low field region only undergo half a gyration in the high field region before being returned to the low field region with oppositely directed velocity, leading to a current layer.

The inner and outer heliosheaths are the regions between the termination shock and the heliopause and between the heliopause and the bow shock/VLISM plasma, respectively. The inner heliosheath is thus filled primarily with shocked solar wind plasma, with the outer heliosheath containing either shocked VLISM plasma or unshocked VLISM plasma depending on whether the bow shock exists or not.

The termination shock, heliopause, bow shock, and inner and outer heliosheaths are the well-accepted global plasma structures expected in the outer heliosphere. Where are they located and what are the properties of their plasmas? Detailed predictions require the use of global gasdynamic (GD) or MHD simulation codes, with or without (ideally with) pick-up ions, or MHD codes. Before describing these results, it is appropriate to provide some approximate estimates of the locations of the heliopause.

The simplest way to estimate these locations is to use the momentum/pressure balance results in Lectures 5, 13, 18 and 19. From Lecture 13:

$$\eta v^2 + P_{th} + \frac{B_t^2}{2\mu_0} = \text{constant} \tag{20.2}$$

where the subscript t means "tangential". A more general equation is

$$\eta v_{sw}^2 + P_{th} + \frac{B_t^2}{2\mu_0} + P_{cr} + P' = \text{constant} \ , \tag{20.3}$$

where P_{cr} is the pressure in cosmic rays and P' represents the pressure in magnetic turbulence, dust, and any other effects [Zank, 1999]. First, balance the solar wind ram pressure against the thermal pressure of the VLISM neutral gas, ignoring the effects of pick-up ions on the solar wind flow:

$$m_i v_{sw}^2 \frac{n_0}{R_{AU}^2} = n_n k_B T_n \ , \tag{20.4}$$

where R_{AU} is the heliocentric distance in AU, n_0 is the solar wind number density at 1 AU, and the subscripts n correspond to the VLISM neutral gas. Substituting in $n_0 \sim 7$ cm^{-3} and $v_{sw} = 400$ km s^{-1} and the quantities in Table 1 yields a characteristic distance

$$R \sim 350 \text{ AU} \tag{20.5}$$

with $P_{th} \sim 10^{-14}$ N m^{-2}.

This estimate varies substantially when other pressures are considered in Eq. (20.2). Adding thermal electrons and protons to the VLISM with the same temperature and with a number density ~ 0.1 cm^{-3} reduces this estimate by a factor $\sim \sqrt{3}$ to about 210 AU. Subsequently adding magnetic pressure in the VLISM, with an estimate of 0.2 nT (they range from $\sim 0.1 - 0.6$ nT), yields a magnetic pressure of $\sim 1.6 \times 10^{-14}$ N m^{-2} and a further decrease in the predicted distance to the heliopause. Note also the theoretical prediction of a factor of 2 increase in magnetic field strength due to the current layer at the heliopause, which multiplies the above magnetic pressure by a factor of 4. Similarly, the canonical estimate for the pressure of cosmic rays in the local ISM is $\sim 10^{-13}$ N m^{-2} [Zank, 1999]. It is thus clear that all the above contributions to the pressure are possibly important and that the associated predictions for location of the heliopause range widely, from numbers $\sim 100 - 200$ AU.

Standard MHD theory predicts that the distance between a bow shock and its magnetopause obstacle should be about $20 - 30\%$ of the distance to the heliopause [e.g., Spreiter et al., 1966]. This suggests that the distance between the termination shock and the heliopause is likely to be at least 20 AU.

Figure 20.3 shows the results of 2-D GD simulations with multiple fluid components for the pick-up ions that originate in different regions [Zank et al., 1996]. The solar wind and VLISM parameters are similar to those in Table 1. Note that in the upwind direction the termination shock and heliopause are about 95 AU and 140 AU from the Sun, respectively, and that they are at greater distances in other directions. These and similar calculations show that neglecting pick-up ions, or varying the description of the pick-up ions, or the inclusion of magnetic field effects do not affect the qualitative nature of these plasma boundaries but do affect their locations and the associated changes in plasma parameters.

Figure 20.4 shows the radial variation of the plasma density in various directions in Figure 20.3 [Zank et al., 1996]. The R^{-2} variation in the solar wind plasma density is clearly seen, as is the step-like increase in plasma density at the termination shock, a small rise in density in the inner heliosheath, the large rise in plasma density at the heliopause, and the subsequent decrease in plasma density beyond the bow shock in the undisturbed VLISM. The heliopause is therefore expected to separate the relatively fast (subsonic), dilute shocked solar wind plasma from the relatively dense but slow plasma of the (shocked?) VLISM. The rapid and large increase in f_p that occurs as a shock or observer moves up and beyond the heliopause is directly relevant to the radio emissions discussed below.

Figure 20.5 shows the predictions of Florinski et al.'s [2004] 3-D axisymmetric 4-species multifluid MHD code. The termination shock, heliopause, and outer bow shock are clearly visible, as is the so-called "hydrogen wall" due to charge-exchange of hydrogen atoms and protons on both sides of the heliopause. The radial variations

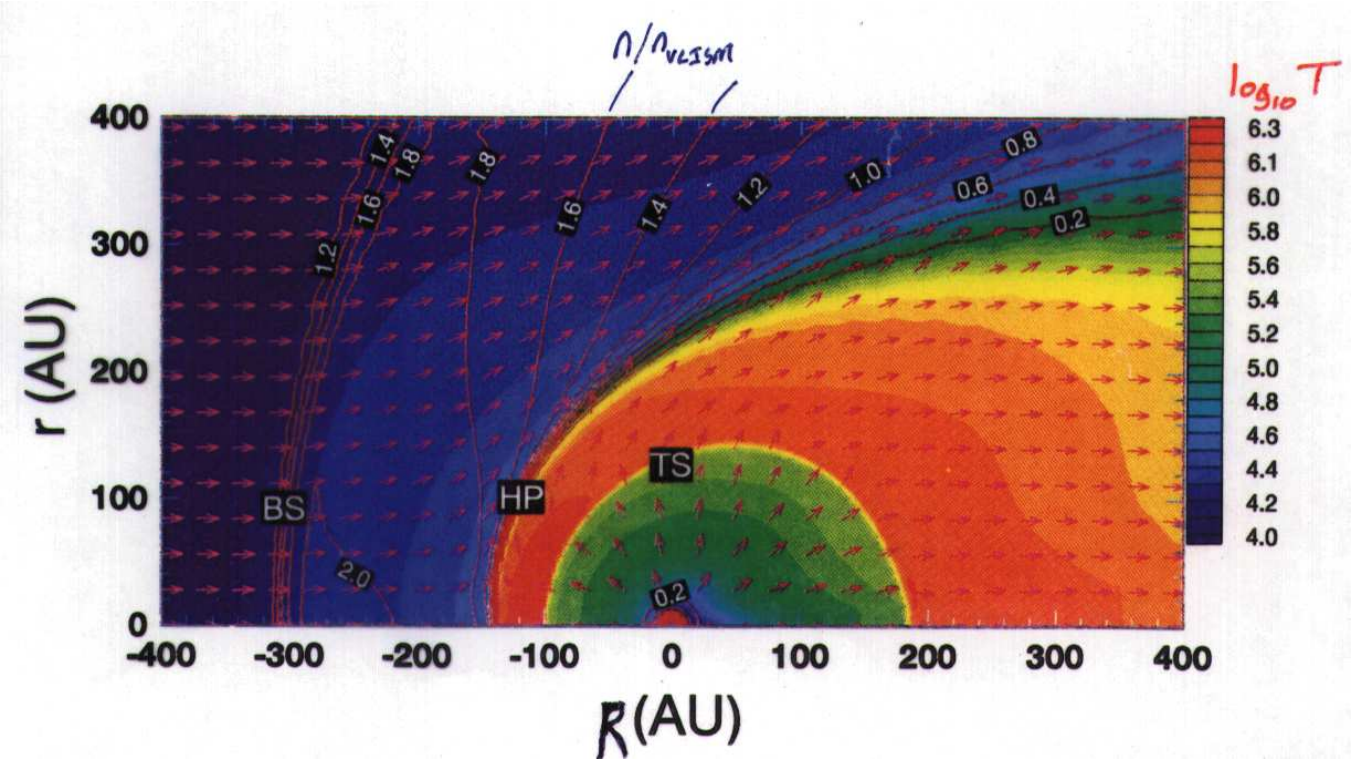

Figure 20.3: Simulation results of Zank et al. [1996] for the temperature (colour coding) and the plasma density relative to the VLISM plasma density (contours), with arrows showing the direction of the plasma flow. The heliopause (HP), termination shock (TS), and bow shock (BS) are clearly visible.

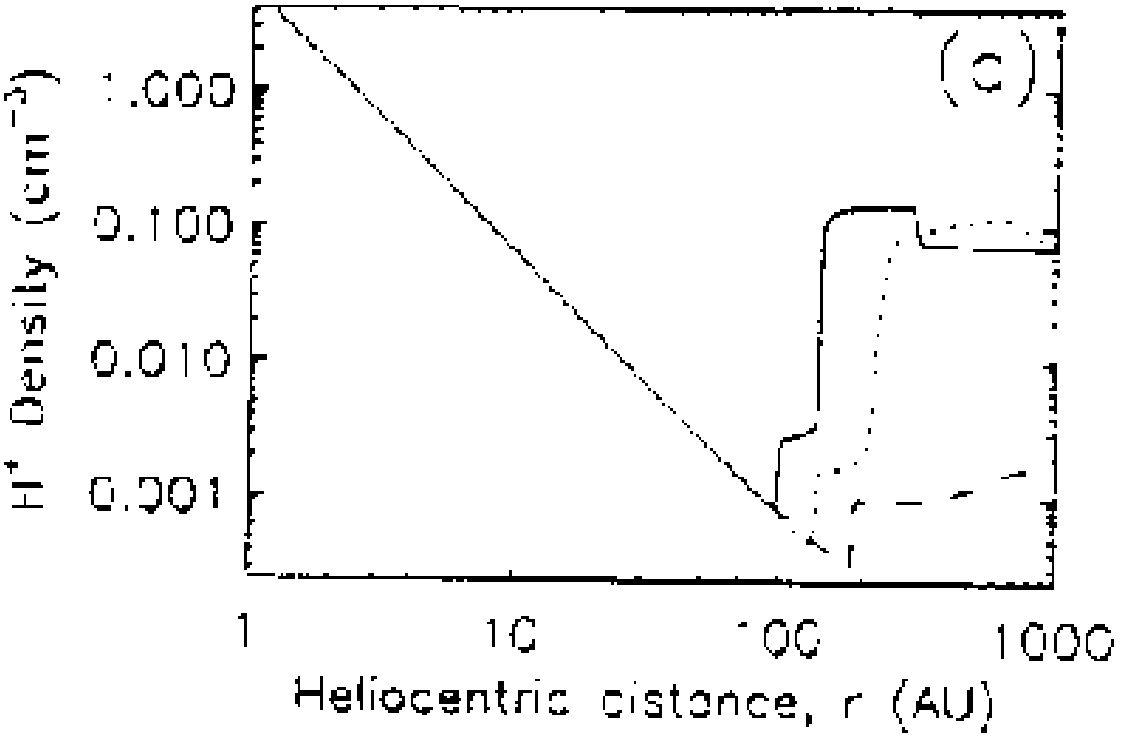

Figure 20.4: Simulation results of Zank et al. [1996] for the plasma density as a function of heliocentric distance in the upwind (full line), transverse (dotted line), and downwind (dashed line) directions. directions.

of the plasma density along various lines of sight are very similar to those in Figure 20.4 [Zank et al., 1996].

20.4 The termination shock

At the lowest level of complexity the termination shock is expected to be a fast mode MHD shock which is attempting to propagate Sunwards against the solar wind flow. It is similar to the roiling, turbulent wave of water in a sink that tries to move back towards the place where the tap's output lands. The termination shock is therefore a reverse shock, so that the upstream side is closest to the Sun and the downstream side is further from the Sun. Accordingly, the solar wind plasma should be compressed, heated, deflected, and slowed across the shock, while the magnetic field should increase. In common with other fast mode shocks, a foreshock region is expected upstream, populated by convected solar wind plasma and charged particles reflected and accelerated at the shock (and in the foreshock by Fermi acceleration processes) and by particles leaking from the heliosheath [Macek et al., 1991]. This foreshock is expected to have the usual types of plasma waves and unstable particle distributions found at planetary foreshocks and in front of travelling interplanetary shocks.

Perhaps the most exciting events of the last decade for NASA's Voyager missions were the crossing of the termination shock on 20 December 2004 for Voyager 1 and around 1 Setepber 2007 for Voyager 2. For Voyager 1 Figure 20.6 shows the upstream accelerated electrons and ions, while Figure 20.8 shows the upstream Langmuir waves associated with undetected electron beams. These characteristics are similar to those expected (although a detailed examination of the particle data yields theoretical difficulties that remain unexplained today). Figure 20.9 shows the magnetic field data. It is clear that the shock has been crossed, unfortunately with only a single crossing that occurred in a data gap!

Very recently Voyager 2 crossed the termination shock with a functioning instrument for detecting the thermal plasma. Figure 20.10 shows the flow speed, number density, temperature, East-West and then North-South flow angles, and the magnetic field strength. Figure 20.11 shows the magnetic field data in more detail. Reasonable accord with previous expectations is apparent until the heating of the solar wind protons is considered: the downstream temperature is of order 10^5 K instead of the values $\approx 10^6$ K expected from (20.2) on balancing the downstream thermal pressure against the solar wind ram pressure. Notice also the significant slowing of the solar wind, with some disordered magnetic activity, in the ≈ 100 days prior to the first shock crossing. These aspects suggest that interstellar pickup ions are playing a vital role, as predicted earlier but not universally accepted [Zank et al., 1996]. In particular, pickup ions have large gyrospeeds compared with the solar wind protons, thereby having a larger fraction with small speeds relative to the shock (and energies small compared with the cross-shock potential) in the vicinity of the shock. These pickup ions will be preferentially reflected by the shock into an ion ring, gyrate upstream for a gyroradius and then move downstream to be thermalized. Put another way, much of the solar wind ram energy is expected to go into the solar wind pickup ions rather than protons in the solar wind core.

The termination shock is believed responsible for the acceleration of the so-called "anomalous" cosmic rays. These are (primarily) singly charged hydrogen, helium, argon, nitrogen, oxygen, and carbon nuclei with energies of order $20 - 300$ MeV. It is believed that these particles are originally interstellar neutrals that are picked-up by the solar wind, convected outward, and energised at the termination shock. The details of this acceleration process are still being worked on. One problem with this idea is that the expected peak in the flux of anomalous cosmic

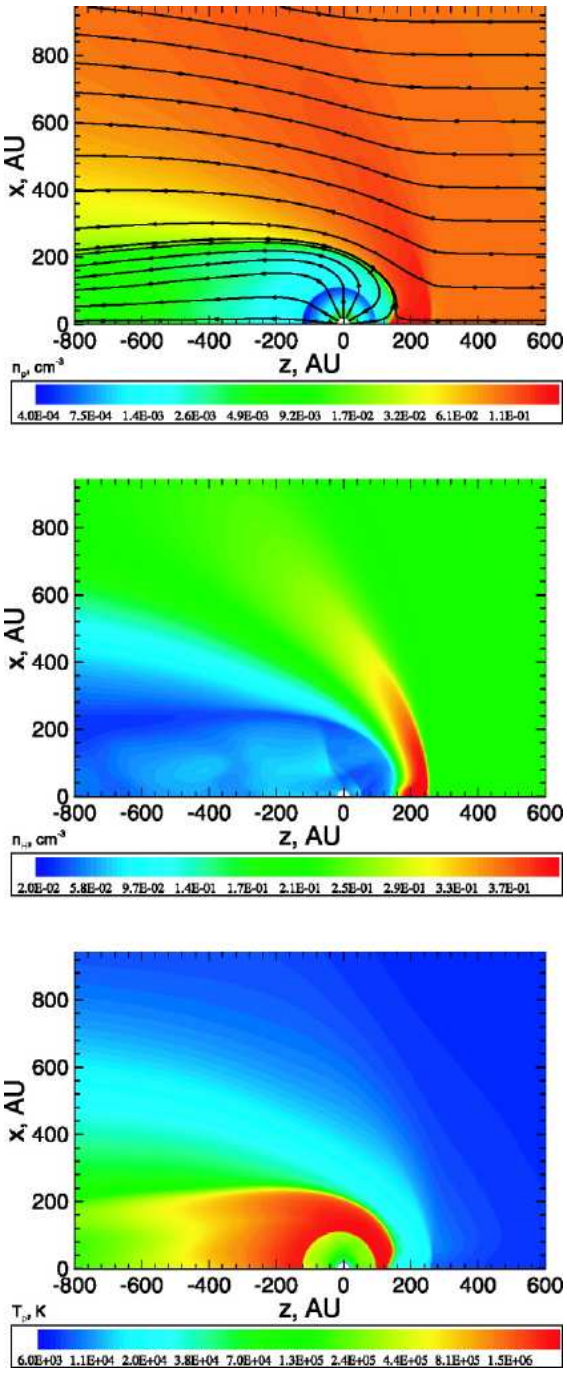

Figure 20.5: Simulation results of Florinski et al. [2004] for the proton number density (top), hydrogen atom number density (middle), and proton temperature (bottom) as a function of location. The Sun is at $(0, 0)$ and the VLISM flows from right to left parallel to the X axis.

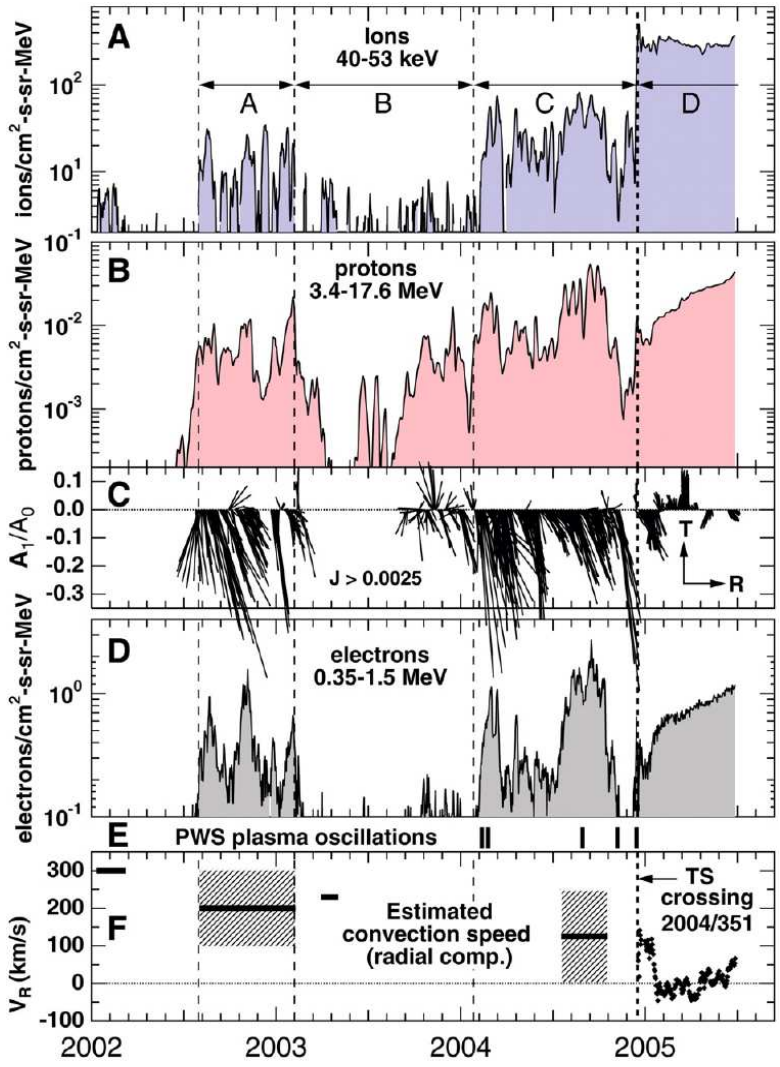

Figure 20.6: Observations by the LECP instrument on Voyager 1 [Decker et al., 2005], showing upstream particles and plasma waves, as well as the slowly varying but higher levels of downstream particles.

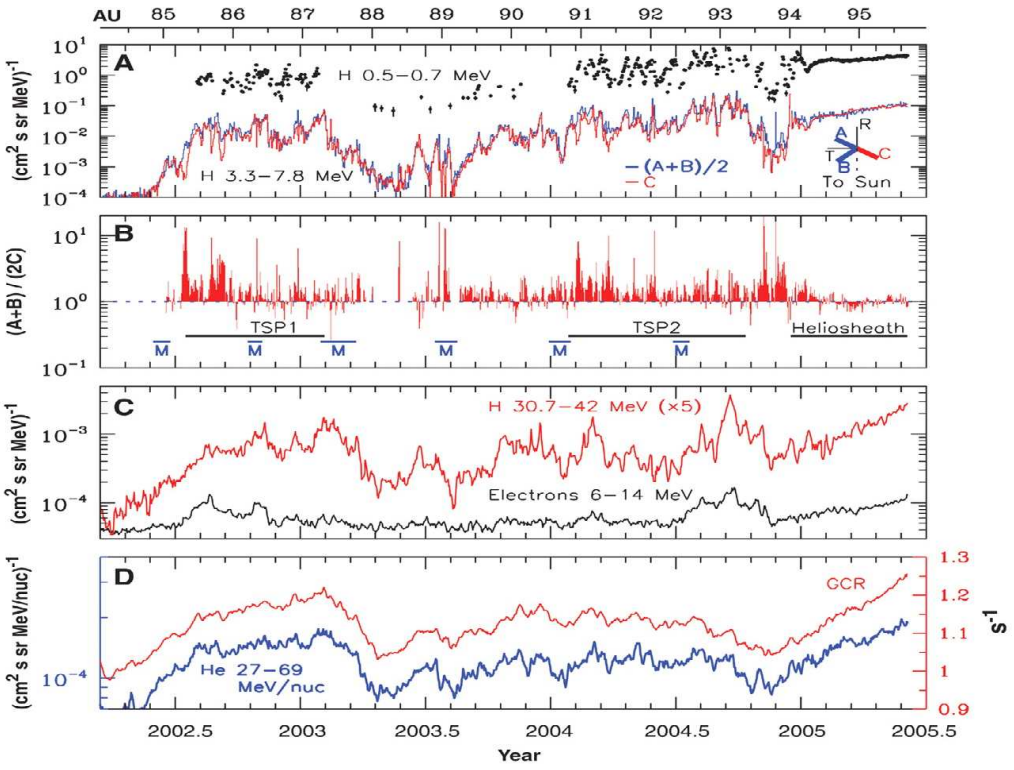

Figure 20.7: Observations by the LECP instrument on Voyager 1 [Stone et al., 2005].

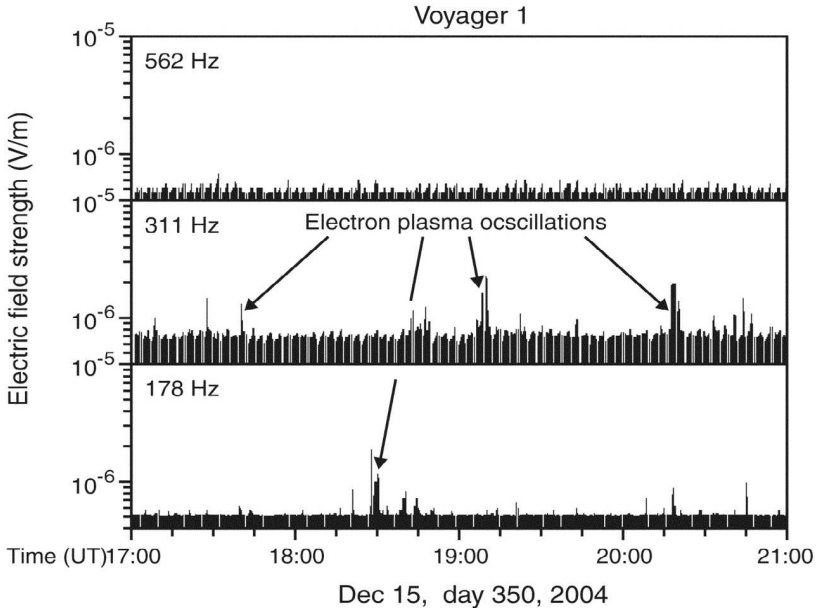

Figure 20.8: Observations by the plasma wave instrument on Voyager 1 [Gurnett and Kurth, 2005].

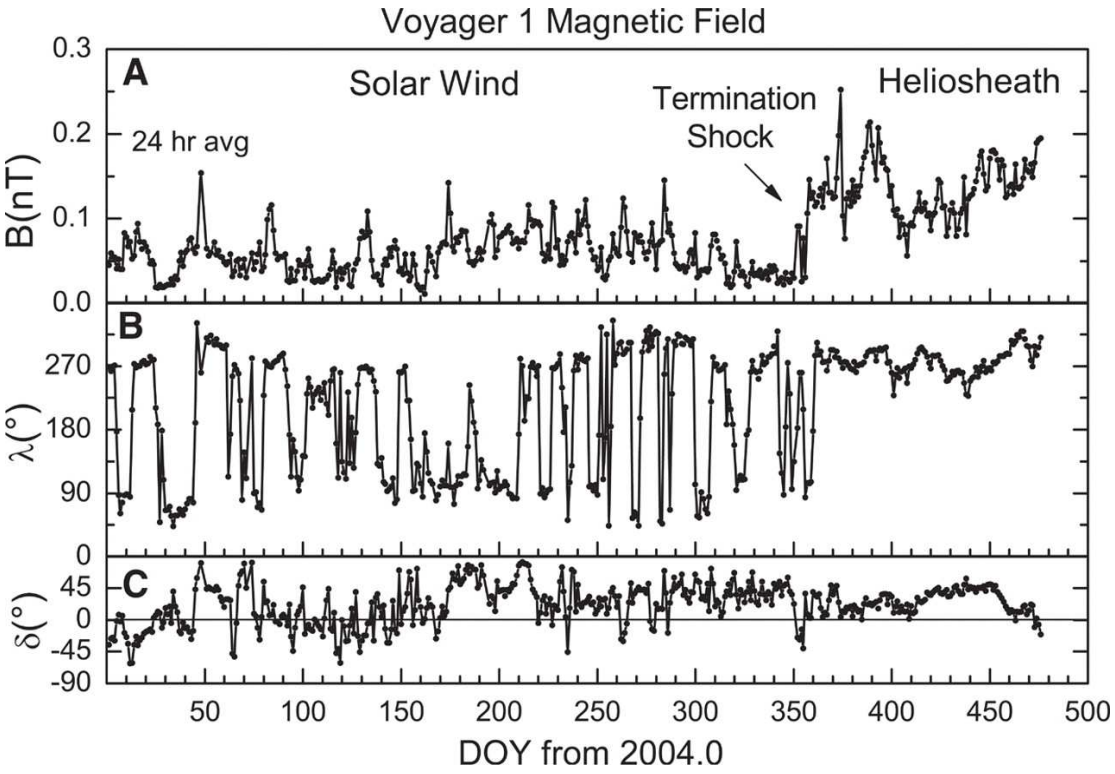

Figure 20.9: Observations by the magnetometer on Voyager 1 [Burlaga et al., 2005].

rays at the termination shock (with a decrease into the solar wind and into the inner heliosheath) has not been observed by Voyager (Figure 20.7. Instead the fluxes appear to be increasing towards the heliopause.

At a more complex level, the anomalous and interstellar cosmic rays may have sufficient energy density to modify the termination shock from being a primarily MHD shock to being a cosmic ray-modified shock, as suggested by the pressure of cosmic rays being comparable to the other pressures in the discussion of Eqs (20.2) and (20.3) [Donohue and Zank, 1993; Zank et al., 1994]. This might affect the detailed shock structure, including the compression ratio of the plasma density on both sides of the shock, and the locations of the shock and heliopause.

20.5 Radio emissions from the outer heliosphere

The first radio emissions observed to come from the outer heliosphere were observed at frequencies of $\approx 2 - 3.5$ kHz by the Voyager spacecraft in 1983 [Kurth et al., 1984]. At this time, the spacecraft were just outside the orbit of Saturn, where the average solar wind plasma frequency is ≈ 2 kHz. Figure 20.12 presents the Voyager 1 plasma wave observations from 1982 until the end of 1993. The radio emissions occurred in three major, sporadic outbursts, one in the period 1983-1984, one in the period 1992-1995, and one in the period 2002-2007, albeit with with several, minor events that are very close to the noise level. (Even the most intense burst is only a factor of ≈ 3 above the instrument noise level.) Two classes of radio emissions are identified: (1) "transient emissions" which drift steadily upward in frequency from ≈ 2.4 kHz to a maximum near 3.5 kHz, over a period of about 180 days; (2) the "2 kHz component" which remains in the frequency range $\approx 1.8 - 2,4$ kHz, shows no frequency drift, and is more uniform, longer-lasting, and slowly varying than the

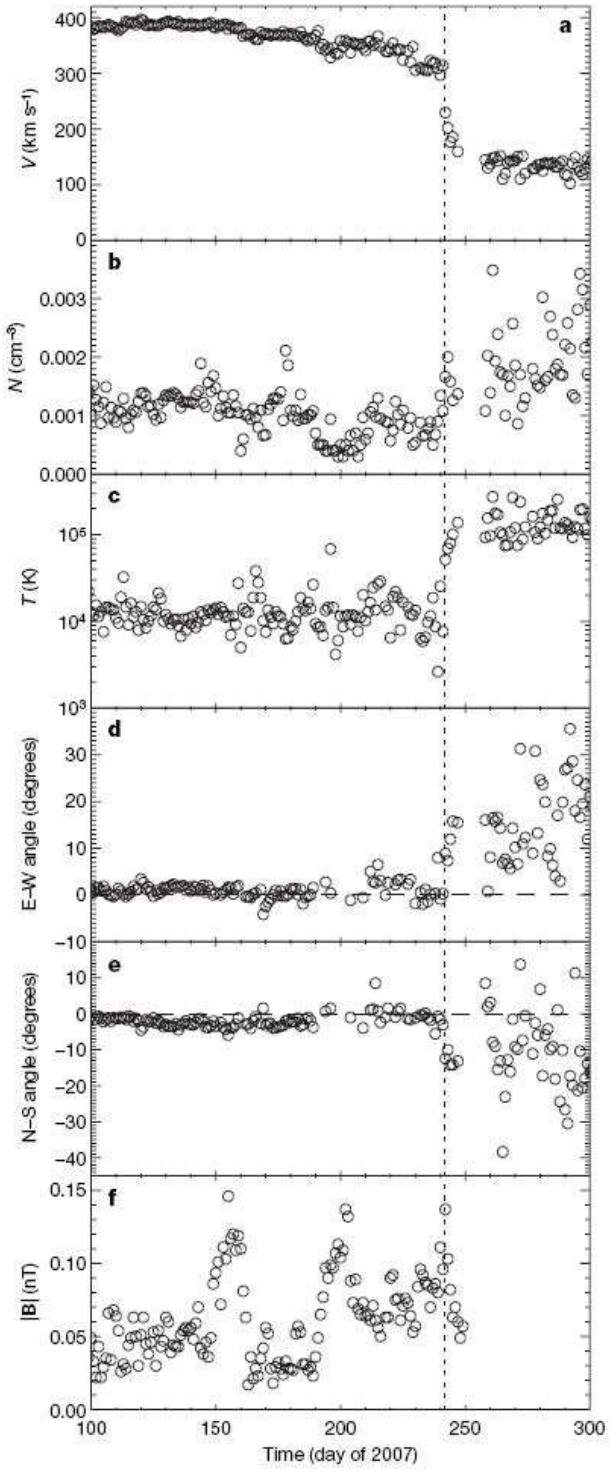

Figure 20.10: Observations of the termination shock by the thermal plasma instrument (PLS) on Voyager 2 [Richardson et al., 2008].

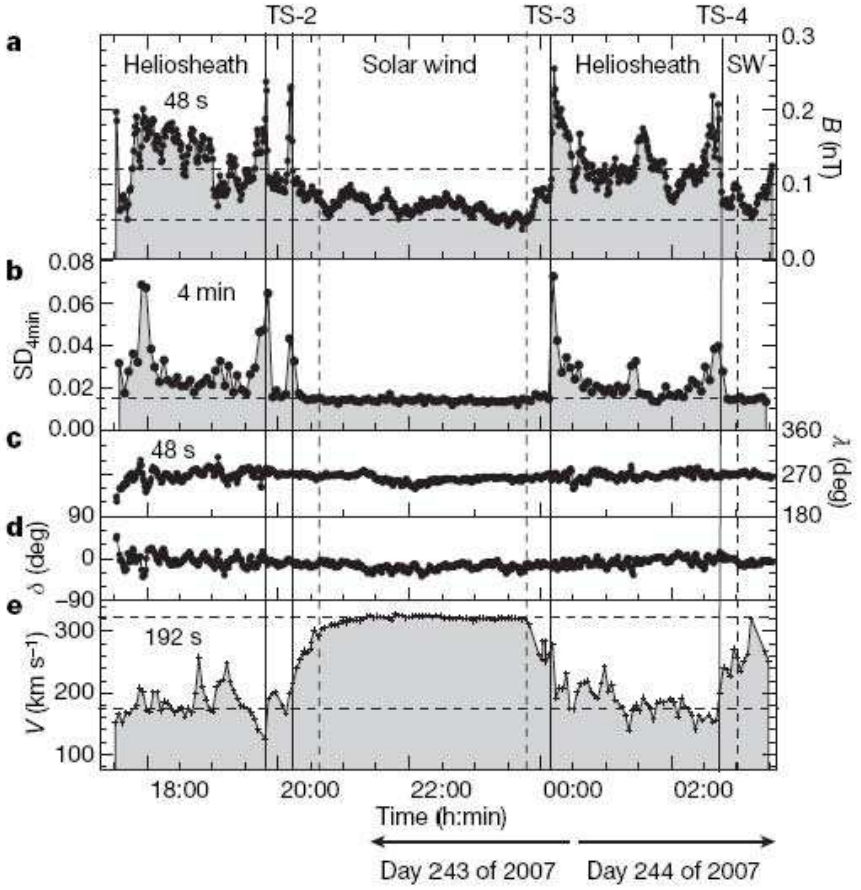

Figure 20.11: Observations of the termination shock by the magnetometer and thermal plasma instrument on Voyager 2 [Burlaga et al., 2008].

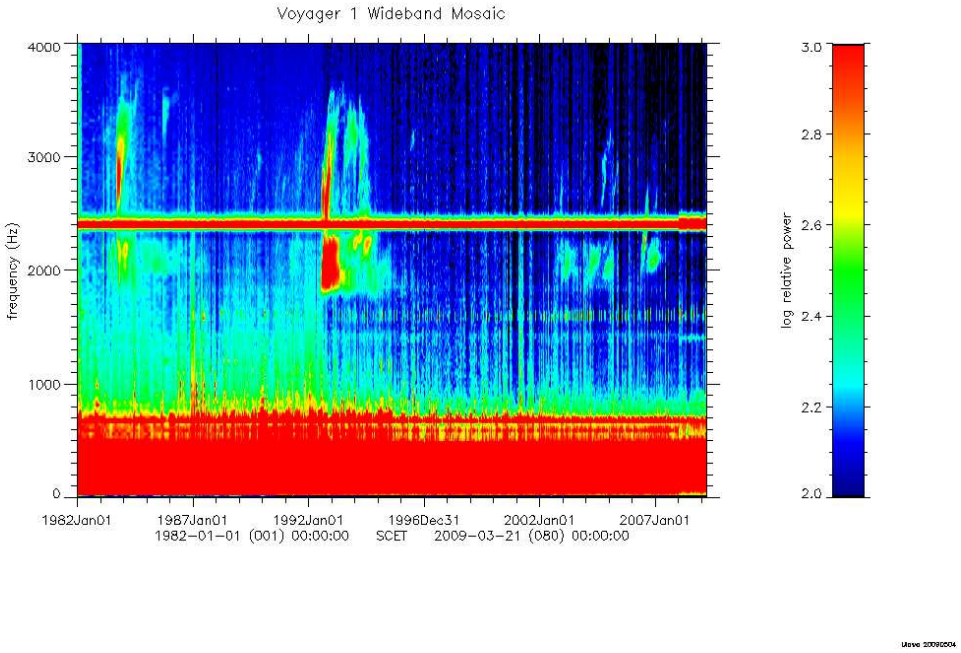

Figure 20.12: Dynamic spectrum of Voyager 1 data, showing the 1983-1984, 1992-1993, and 2002-2007 outbursts of radiation from the outer heliosphere [Gurnett and Kurth, 1995; http://www-pw.physics.uiowa.edu/ wsk/vgr/recent.html, October 2008]. The dark, very uniform band from $\sim 2.3 - 2.4$ kHz is interference from the spacecraft power supply.

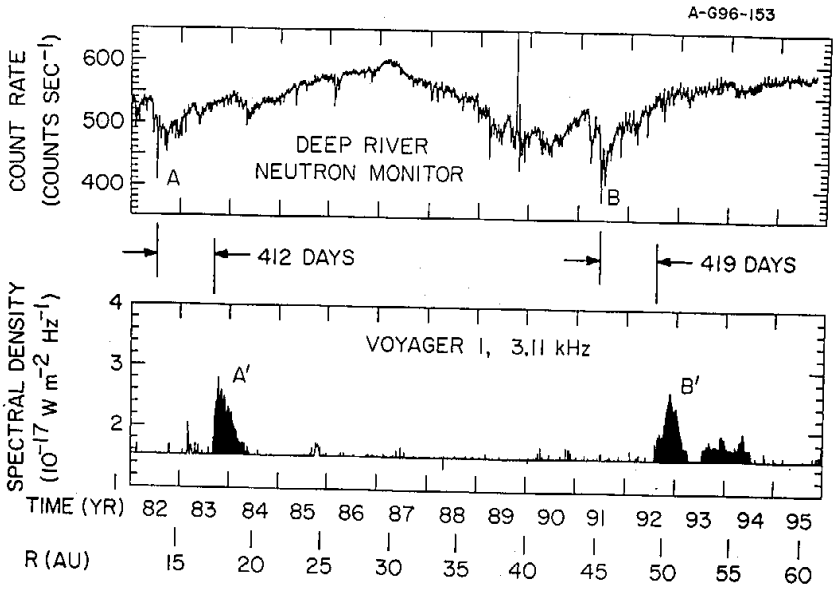

Figure 20.13: Cosmic ray counts from the Deep River Neutron Monitor are compared with the flux densities of the outer heliospheric radiation measured by Voyager 1 [Gurnett and Kurth, 1995].

transient emissions.

These are the most powerful radio emissions in our solar system, having a total power $\geq 10^{13}$ W. This power is greater than that in Jovian radio emissions ($\sim 10^{11}$ W), the Earth's AKR ($\sim 10^{9}$ W), and type III solar radio bursts. The most likely sources of this power are (i) the solar wind's ram energy or (ii) transient shocks engendered by solar activity. (VLISM shocks are unlikely given the approximately solar-cycle periodicity of the major radiation events.

The emissions were quickly interpreted in terms of a source in the outer heliosphere beyond the planets, based on Voyager observations in the Jovian and Saturnian magnetospheres, the frequencies and intensity of the emissions, and the appearance of the emissions only after the average value of f_p in the solar wind decreased below about 2 kHz [e.g., Kurth et al., 1984; Macek et al., 1991]. Indeed the foreshock region sunward of the termination shock was considered in detail as the source of the radiation [e.g., Macek et al., 1991; Cairns and Gurnett, 1992], with the theory involving foreshock electron beams, Langmuir waves and the production of f_p and $2f_p$ radiation as in type III solar radio bursts and Earth's $2f_p$ radiation (Lectures 9, 10, and 13) . This proposed source region is now considered most unlikely due to f_p falling off as R^{-1} in the solar wind, with $f_p \sim 250$ Hz at 100 AU on average, making it very difficult to produce radiation at frequencies of $2 - 4$ kHz with this emission mechanism.

Figure 20.13 [Gurnett and Kurth, 1995] provides strong evidence for McNutt's [1988] idea that the radio events are triggered by solar wind disturbances when they reach the vicinity of the termination shock and heliopause. The figure shows that each major radio event follows ≈ 415 days after one of the two largest decreases in the cosmic ray flux observed at Earth (Forbush decreases), both of which were associated with periods of unusually high solar activity and multiple CMEs. Figure 20.14 demonstrates that a global disturbance developed in the distant solar wind and then propagated further out [Gurnett et al., 1993]. This global disturbance results from the merging of multiple CMEs and associated shocks and magnetic

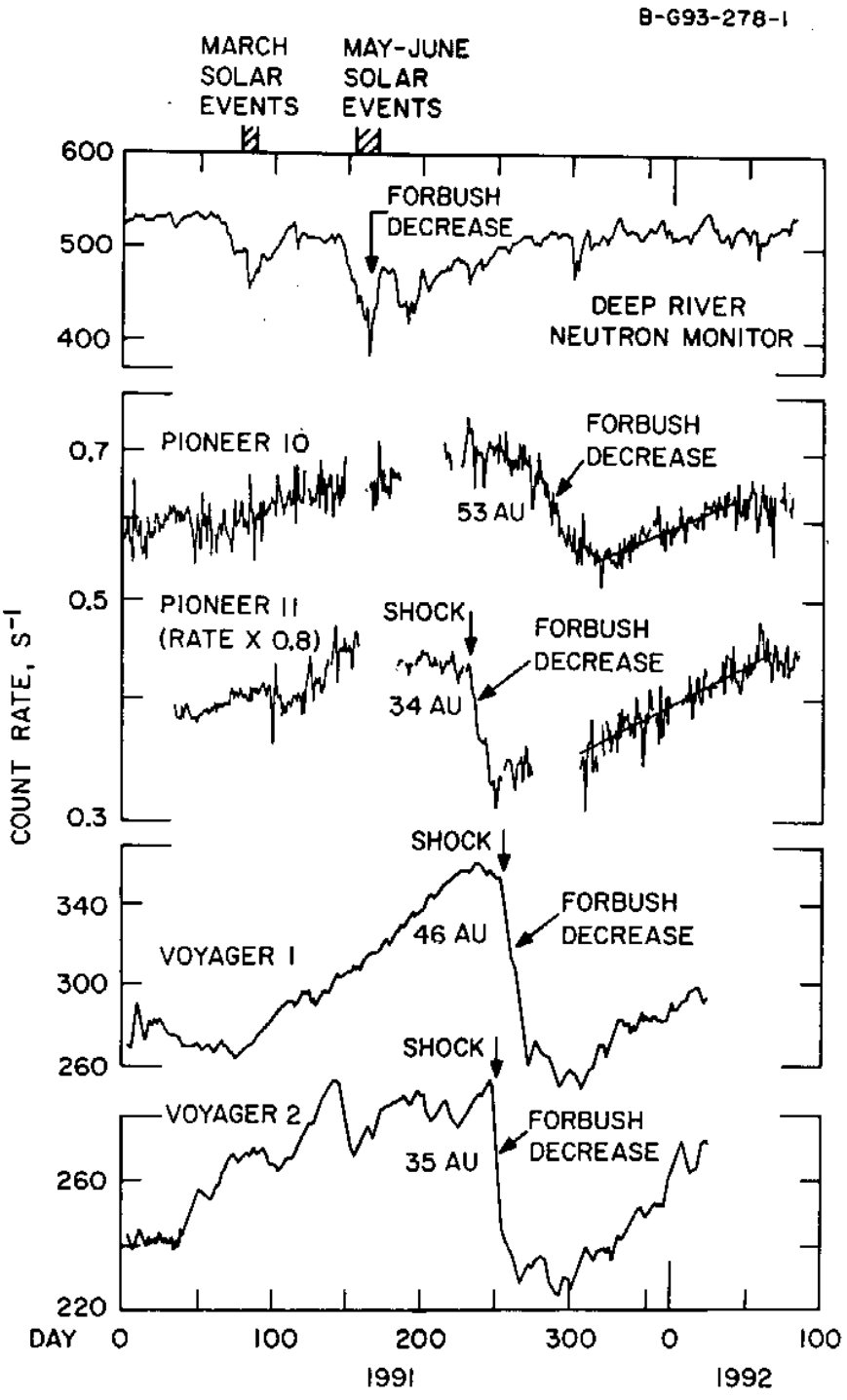

Figure 20.14: Cosmic ray counts from the Deep River Neutron Monitor and the Pioneer and Voyager spacecraft are compared as functions of heliocentric distance and time for the disturbance that apparently triggered the 1992-1993 radio emissions [Gurnett et al., 1993].

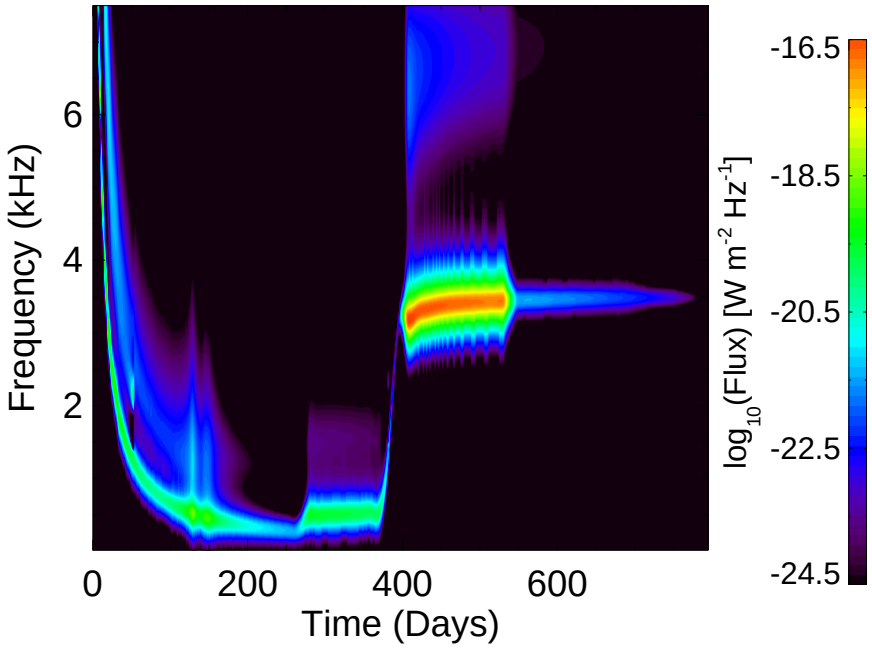

Figure 20.15: Dynamic spectrum of f_p and $2f_p$ radiation generated upstream of a shock moving with constant isotropic speed through the 3-D plasma density structures shown in Figures 20.3 and 20.4 [Mitchell et al., 2004].

field enhancements into a single entity, called a "global merged interaction region" (GMIR). This GMIR, at least, is preceded by a shock wave (Figure 20.14). Taking the shock speeds v_{sh} for the GMIRs associated with the two radiation events, $\approx 810 - 850$ km s^{-1}, and the time delay Δt between the onset of the radiation and the Forbush decrease at Earth the distance to the source can be estimated from the obvious equation

$$R = v_{sh}\Delta t \ . \tag{20.6}$$

Substituting these numbers into the equation yields $R \sim 190 - 200$ AU. Correcting for the change in shock speed across the shock, yields $R \sim 110 - 180$ AU [Gurnett et al., 1993].

Gurnett et al.'s [1993] model for the radio emissions therefore involves the GMIR shock starting to produce f_p and $2f_p$ radiation after it traverses the heliopause, with the transient emissions coming from a putative density enhancement near the nose of the heliopause, while the 2 kHz component comes from other regions of the outer heliosheath. This model can be tested directly using the plasma density structures obtained from modern global simulations of the outer heliosphere. Figure 20.13 shows the dynamic spectrum predicted for a GMIR shock that produces f_p and $2f_p$ radiation in an upstream foreshock as it moves through the global 3-D density structures obtained from Zank et al.'s [1996] simulation code [Mitchell et al., 2004]. A number of emissions can be identified in Figure 20.15. First, the emissions that drift from above 6 kHz to about 300 Hz near day 300 are f_p and $2f_p$ emission from the undisturbed solar wind. Second, emission from the inner heliosheath is seen from days 300 to 400 from about 200-500 Hz. Third, the emissions drifting rapidly from $\sim 0.2 - 3.5$ kHz are associated with the shock moving up the density ramp at the heliopause. Fourth, the intense, uniform and slow varying emissions with constant frequencies ~ 3.5 kHz are produced at f_p when the shock is in the

outer heliosheath beyond the heliopause. (The $2f_p$ radiation is orders of magnitude weaker. Indeed, only the outer heliosheath emission is above the Voyager detection threshold of about 10^{-17} W m^{-2}Hz^{-1}.) Note that current best estimates of f_p in the VLISM yield $f_p \sim 1.5 - 3.5$ kHz.

Comparing Figures 20.12 and 20.15, it is very appealing to interpret the 2 kHz component as f_p radiation from the outer heliosheath, consistent with Gurnett et al.'s [1993] model. Unfortunately, however, the only drifting emissions in Figure 20.13 occur when the shock drifts up the heliopause density ramp and occur far too rapidly to be consistent with the observed time scale for the transient emissions ($\sim$ 180 days).

At the present time, then it appears that a reasonable theoretical explanation exists for one of the two observed classes of radiation but not for the second class [Mitchell et al., 2004]. For phenomena that lie on the true border between astrophysics and space physics this is not unexpected. A number of teams are working on this radiation and the plasma environment of the outer heliosphere. Further progress is therefore expected.

20.6 Concluding remarks

Hopefully, in the next few years, as you make your paths in the world as newly-fledged Honours, Masters, or PhD graduates you will find that the physics and topics covered in this course remain interesting and perhaps useful to you. You have learnt about solar physics, the interplanetary medium, Earth's magnetosphere and ionosphere, other planetary magnetospheres, space weather effects, and the outer heliosphere. This has required you learning much plasma physics, in particular about (i) single particle motions, (ii) shock waves, (iii) current layers, (iv) MHD and fluid physics, (v) kinetic physics, (vi) plasma waves and radiation, (vii) acceleration and heating processes, and (viii) wave-particle interactions. This knowledge and set of skills should be useful in fields ranging from plasma physics to atmospheric physics to space physics and astrophysics.

Let me say that I have enjoyed teaching you and that I hope that you have enjoyed yourselves and learnt useful things. Please feel free to talk with me on any aspect of the course and on space science, both before and after the final exam.

20.7 References and Bibliography

- Burlaga, L., et al., Crossing the termination shock into the heliosheath: Magnetic fields, **Science**, **309**, 2027, 2005.
- Burlaga, L., et al.,Magnetic fields at the solar wind termination shock, **Nature**, **454**, 75, 2008.
- Cairns, I.H., and D.A. Gurnett, Outer heliospheric radio emissions 1. Constraints on emission processes and the source region, **J. Geophys. Res.**, **97**, 6235, 1992.
- Decker, R.B., et al., Voyager 1 in the foreshock, termination shock, and heliosheath, **Science**, **309**, 2020, 2005.
- Donohue, D.J., and G.P. Zank, The steady-state and dynamical structure of a cosmic-ray-modified termination shock, **J. Geophys. Res.**, **98**, 19,005, 1993.
- Frisch, P.C., Boundary conditions of the heliosphere. **J. Geophys. Res.**, **108(10), LIS 11-1, 2003.**

- **Gurnett, D.A., and W.S. Kurth, Heliospheric 2-3 kHz radio emissions and their relationship to large Forbush decreases, Adv. Space Res., 16(9), 279, 1995.**
- **Gurnett, D.A., and W.S. Kurth, Electron plasma oscillations upstream of the solar wind termination shock, Science, 309, 2027, 2005.**
- **Gurnett, D.A., W.S. Kurth, S.C. Allendorf, and R.L. Poynter, Radio emission from the heliopause triggered by an interplanetary shock, Science, 262, 199, 1993.**
- **Kurth, W.S., D.A. Gurnett, F.L. Scarf, and R.L. Poynter, Detection of a radio emission at 3 kHz in the outer heliosphere, Nature, 312, 27, 1984.**
- **Lallement, R., Measurements of the interstellar gas, in** *Observations of the Outer Heliosphere*, **Ed. D.E. Page, Adv. Space Res., 13(6), 113, 1993.**
- **Linsky, J.L., A. Brown, K. Gayley, et al., Astrophys. J., 402, 694, 1993.**
- **Macek, W.M., I.H. Cairns, W.S. Kurth, and D.A. Gurnett, Plasma wave generation near the inner heliospheric shock, Geophys. Res. Lett., 18, 357, 1991.**
- **McNutt, R.L., Jr., A solar-wind "trigger" for the outer heliospheric radio emissions and the distance to the terminal shock, Geophys. Res. Lett., 15, 1307, 1988.**
- **Mitchell, J.J., I.H. Cairns, and P.A. Robinson, Theory for 2-3 kHz radiation from the outer heliosphere, J. Geophys. Res., 109, A06108, 2004.**
- **Spreiter, J.R., A.L. Summers, and A.Y. Alksne, Hydromagnetic flow around the magnetosphere, Planet. Space Sci., 14, 223, 1966.**
- **Stone, E.C., et al., Voyager 1 explores the termination shock region and the heliosheath beyond, Science, 309, 2017, 2005.**
- **Richardson, J.D., et al., Cool heliosheath plasma and deceleration of the upstream solar wind at the termination shock, Nature, 454, 63, 2008.**
- **Witte, M., M. Banaszkiewicz, and H. Rosenbauer, Space Sci. Rev., 78, 289, 1996.**
- **Zank, G.P., Interaction of the solar wind with the local interstellar medium: A theoretical perspective, Space Sci. Rev., 89 (3/4), 1, 1999.**
- **Zank, G.P., I.H. Cairns, D.J. Donohue, and W.H. Matthaeus, Radio emissions and the heliospheric termination shock, J. Geophys. Res., 99, 14,729, 1994.**
- **Zank, G.P., H.L. Pauls, L.L. Williams, and D.T. Hall, Interaction of the solar wind with the local interstellar medium: A multifluid approach, J. Geophys. Res., 101, 21,639, 1996.**